



Enabling comprehensive assessment of marine eutrophication impacts and their evaluation against regional safe operating space

Eldbjørg Blikra Vea¹ · Mark Jwaideh² · Katherine Richardson³ · Morten Ryberg⁴ · Anders Bjørn¹ · Michael Hauschild¹

Received: 24 October 2023 / Accepted: 10 April 2024
© The Author(s) 2024

Abstract

Purpose Nitrogen emissions from human activities are contributing to elevated levels of eutrophication in coastal ecosystems. Mechanisms involved in marine eutrophication show strong geographical variation. Existing life cycle impact assessment (LCIA) and absolute environmental sustainability assessment (AESA) methods for marine eutrophication do not adequately represent this variability, do not have a full global coverage, and suffer from other limitations, such as poor estimation of coastal residence times. This study aims to advance LCIA and AESA for marine eutrophication.

Methods We aligned and combined recent advancements in marine eutrophication LCIA and AESA methods into one method. By re-running models underlying the combined methods and incorporating additional data sources, we included marine regions missing in previous methods and improved fate modeling, with the inclusion of denitrification and plant uptake in the air emission-terrestrial deposition pathway. To demonstrate and validate our method, we applied it in a case study.

Results The developed method allows the assessment of marine eutrophication impacts from emissions to soil, freshwater, and air at high resolution (0.083° and $2^\circ \times 2.5^\circ$ for inland and air emissions, respectively) and spatial coverage (all ice-free global continents). In the case study, we demonstrate the added value of our method by showing that the now quantified spatial variability within spatial units, e.g., river basins, can be large and have a strong influence on the modeled marine eutrophication from the case study. Compared to existing methods, our method identifies larger occupations of safe operating space for marine eutrophication, mainly due to the high resolution of the coastal compartment, reflecting a more realistic areal extent of marine eutrophication impacts.

Conclusions Although limited by factors such as simulations based on a single reference year for modeling inland and air fate, our method is readily applicable to assess the marine eutrophication impact of nitrogen emitted to any environmental compartment and relate it to the safe operating space. With substantial advancement of existing approaches, our method improves the basis for decision-making for managing nitrogen and reducing emissions to levels within the safe operating space.

Keywords Marine eutrophication · Absolute sustainability · Nitrogen emission · Planetary boundaries · Life cycle impact assessment · Life cycle assessment

1 Introduction

An escalating global production of food and energy has led to an increase of nitrogen emissions from applying fertilizers and manure and burning fossil fuels (Beusen

and Bouwman 2022). Consequently, increasing amounts of nitrogen are transported to freshwater bodies and coastal waters (Beusen et al. 2016), causing eutrophication impacts. Marine eutrophication refers to the ecosystem response to input of excess nutrients in the coastal water, causing excessive algal growth, leading to oxygen decline at the seabed in bottom layers and, ultimately, altering

Communicated by Ian Vázquez-Rowe.

✉ Eldbjørg Blikra Vea
ebve@dtu.dk

¹ Center for Absolute Sustainability, Section for Quantitative Sustainability Assessment, Department Environmental and Resource Engineering, Technical University of Denmark, Kongens Lyngby, Denmark

² Institute for Sustainable Resources, University College London, London, UK

³ Center for Macroecology, Evolution and Climate, Globe Institute, University of Copenhagen, Copenhagen, Denmark

⁴ Sweco Danmark A/S, Copenhagen, Denmark

the ecosystem balance (EC-JRC 2010). The loss of oxygen in coastal waters is a leading threat to coastal marine ecosystems (Breitburg et al. 2018; Diaz and Rosenberg 2008; Johnson et al. 2021). Improved and reliable tools are needed for scientists and decision-makers to address the challenges of eutrophication (Morelli et al. 2018).

Life cycle assessment (LCA) is a tool to evaluate environmental impacts (such as marine eutrophication) of a product or process across its lifecycle. In an LCA, life cycle impact assessment (LCIA) methods can be used to calculate characterization factors that translate quantified inputs and outputs of the product system into potential impacts (Hauschild and Huijbregts 2015). LCIA methods consist of characterization factors (CFs) which are the product of a fate factor (FF), exposure factor (XF), and effect factor (EF). These combine to link a substance's emission to its impacts along an impact pathway (i.e., the cause-effect chain from emission to impact). Marine eutrophication is a regional environmental problem, meaning that impact pathway elements are prone to spatial variability (Henryson et al. 2018; Wowra et al. 2020) and that impacts usually happen relatively close to emission sources. Variability arises notably in fate factors (FFs) (Henderson et al. 2021; Henryson et al. 2018; Payen et al. 2021), representing quantitative modeling of the environmental fate of nitrogen compounds and accounting for nitrogen removal in its journey from emission source to the receiving compartment. Multiple factors contribute to this spatial variability. For example, soil retention depends on factors like soil type and weathering, while ocean currents and bathymetry influence coastal residence time.

The spatially differentiated LCIA method of Cosme and Hauschild (2017) is recognized as the best available LCIA method for marine eutrophication (Morelli et al. 2018; UNEP 2019). However, it suffers from several limitations. One concern lies in level of spatial differentiation of the inland fate component that models export of nitrogen compounds from soil and freshwater to coastal water. The inland fate component relies on the global Nutrient Export from WaterSheds (NEWS) 2 model that operates at river basin resolution. Particularly in larger river basins with varying fate mechanisms, this coarse river basin resolution can potentially reduce accuracy (Henderson et al. 2021; Payen et al. 2021; Zhou et al. 2022). Moreover, at least one inland fate component (commonly the fraction exported from soil) is lacking for 680 of 5773 watersheds due to missing input data in NEWS 2, (Bjørn et al. 2020b). In relation to the coastal fate component, modeling the persistence of nitrogen in the coastal compartment, the LCIA method of Cosme and Hauschild (2017) relies on few and uncertain data about coastal water residence times in the 66 large marine ecosystems (LMEs) that it covers (Cosme and Hauschild 2017; Morelli et al. 2018; Veal et al. 2022).

In addition, the method of Cosme and Hauschild (2017) is missing fate and impact models for airborne emissions of nitrogen compounds and is limited to 66 LMEs (Morelli et al. 2018). Finally, the method excludes certain coastal areas that are not considered within the LME definition such as the northern Wharton Basin and Western Pacific Warm Pool (Morelli et al. 2018).

Since the publication of Cosme and Hauschild (2017) method, various studies have contributed with important improvements to marine eutrophication modeling which address several of the limitations mentioned above. Jwaideh et al. (2022) and Zhou et al. (2022) increased the spatial resolution of the inland fate component from river basins to 0.083 and 0.5°, respectively, and created a complete set of FFs for soil and freshwater nitrogen emissions based on the global nutrient model, IMAGE-GNM (Beusen et al. 2015). Zhou et al. (2022) focused only on the fate and transport to freshwater systems, while Jwaideh et al. (2022) also covered transport to the marine environment. Veal et al. (2022) improved the marine fate modeling by introducing refined estimates on coastal water residence time based on Liu et al. (2019), ensuring consistent residence time estimates with high resolution and global coverage. Bjørn et al. (2020b) and Henderson et al. (2021) integrated atmospheric fate modeling from Roy et al. (2012) with Cosme and Hauschild (2017) developing a spatially resolved method allowing to quantify impacts caused by nitrogen emissions to air.

In addition to integrating air emissions into marine eutrophication LCIA modeling, Bjørn et al. (2020a, b, c) introduced an absolute environmental sustainability assessment (AESA) method. This AESA method allows for the comparison of impact estimates with regional safe operating spaces in coastal waters, defined as the difference between threshold values and reference values for oxygen concentrations. AESA builds on LCA, as it assesses the environmental impact of an activity (product or system) and compares this impact to an assigned environmental safe operating space (SOS) delineated by biophysical limits such as the planetary boundaries (Richardson et al. 2023; Rockström et al. 2009; Steffen et al. 2015). The purpose of AESA is to assess if an activity's environmental impacts exceed its allocated share of the SOS and thereby qualify as unsustainable (Bjørn et al. 2020a). In relation to the SOS, the marine eutrophication AESA method of Bjørn et al. (2020b) has a resolution of the coastal compartment that is too coarse (being based on the LMEs of the Cosme and Hauschild (2017) method) to reflect the geographical variability in the SOS adequately. This coarse resolution introduces the risk of overlooking the potential exceedance of regional scale SOS due to the inherent averaging of impacts and thresholds over relatively large coastal areas. Moreover, Bjørn et al. (2020b) assumed that natural reference oxygen conditions (used to calculate the SOS) correspond to an oxygen saturation of 100% in the benthic zone, which is not realistic in all coastal areas (Bjørn

et al. 2020b; Veá et al. 2022). Veá et al. (2022) improved the estimation of SOS by refining the marine compartment’s resolution and adjusting relevant parameters to this scale, including the natural oxygen concentration.

This study aims to unify recent advances in marine eutrophication LCIA and AESA methods into a single and consistent method with a global coverage (i.e., extending coastal coverage beyond 66 LMEs). The new method covers emissions of nitrogen compounds to air, soil, freshwater, and coastal water and their marine eutrophication impact, allowing for comparisons to regional SOS. The new marine eutrophication method is applied to a case study with a highly spatialized inventory to demonstrate its application and compare it to existing methods.

2 Method

2.1 Development—characterization factors

As illustrated in Fig. 1, this study adapted and integrated residence time in coastal waters (T), exposure factors (XF), and SOS as presented in Veá et al. (2022) with fractions exported (FE) to coastal water of a nitrogen compound emitted to soil or freshwater based on Jwaideh et al. (2022), or to air based on Roy et al. (2012). In addition, we included the fraction of plant uptake (FPU), reflecting the removal by

vegetation of nitrogen that is deposited on agricultural land based on Schulte-Uebbing et al. (2022a, b).

2.1.1 Characterization framework

The parameters illustrated in Fig. 1 constitute components of the CFs for emissions to air, soil, freshwater, or coastal water emissions that were calculated according to Eqs. 1 and 2. Note that these CFs cover the cause-effect chain from nitrogen emission to reduced O_2 concentration in coastal bottom waters, hence spanning the FF and XF of the LCIA framework. This allows comparison of the estimated reduction in O_2 concentration to regional SOS within an AESA. As this comparison is the focus here, an EF (though useful in other contexts) is not required.

Equation 1 links the emission to an environmental compartment (coastal water, freshwater, or soil), with its impacts in coastal water subsegments:

$$CF_{i,ss}^m = FF_{ij}^m \times XF_{ss} = FE_{ij}^m \times T_j \times XF_{ss} \tag{1}$$

where.

- $CF_{i,ss}^m \left(\frac{kgO_2}{kgN_j/year} \right)$ translates the emission to compartment m in cell i that is exported to marine receptor cell j , leading to a decrease in oxygen levels in the benthic zone of subsegment ss encompassing cell j .

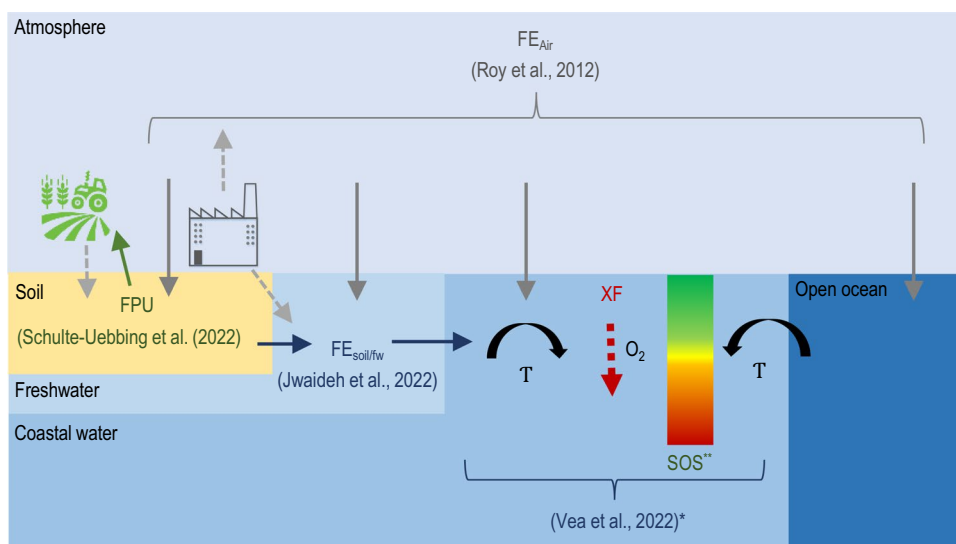


Fig. 1 Overview of the marine eutrophication characterization factor (CF) model and its key parameters. The CFs combine fractions exported ($FE_{soil/fw}$) from soil and freshwater to coastal water (blue arrows), atmospheric fractions exported (FE_{air}) expressing the fraction (dimensionless) of an air emission (NO_x or NH_x) that deposits on any spatial unit (gray arrows), a fraction of plant uptake (FPU) reflecting the fraction of nitrogen depositing on soil that is taken up by vegetation (green arrow), marine fate component (T) expressing

nitrogen residence time in coastal water (black arrow), exposure factors (XF) translating presence of nitrogen in the coastal water subsegment to a decrease in oxygen in the benthic zone (red stippled arrow), and safe operating space (SOS) reflecting the difference between a boundary for minimum O_2 levels and the natural reference level of O_2 . *Builds on Cosme and Hauschild (2017) and Bjørn et al. (2020b) methods. ** SOS is not a part of the CFs but is used in AESA

- $FE_{i,j}^m \left(\frac{kgN_j}{kgN_i} \right)$ is the fraction of the emissions to compartment m in cell i that is exported to marine receptor cell j .
- $T_j \left(\frac{kgN_{ss}}{kgN_j/year} \right)$ is the residence time of nitrogen exported to marine receptor cell j in the coastal water subsegment (defined by the 200-m isobath) before it exits to the open ocean.
- $XF_{j,ss} \left(\frac{kgO_2}{kgN_{ss}} \right)$ is the exposure factor, i.e., the oxygen decrease in the benthic zone in response to the presence of nitrogen in coastal waters in the marine subsegment ss associated with the marine receptor cell j .

The product of $FE_{i,j}^m$ and T_j constitutes the FF of the CFs, representing the inland and marine fate components, respectively. Figure 2A illustrates the spatial link between an inland emission (emission to soil or freshwater) and the geographical location of its associated impact. The coastal area where the marine eutrophication impacts take place depends on which river basin emission cell i is located in and the location of the associated marine receptor cell j , which corresponds to the cell where the river mouth of the specific river basin is located. The marine receptor cell j is situated in a coastal large marine ecosystem (cLME) subsegment ss , which is the estimated area in which a nitrogen emission can propagate and cause eutrophication impacts. Refer to Vea et al. (2022) for more details on the cLME subsegments.

Figure 2B illustrates the spatial link between emissions to air in cell i and their deposition in cell k , which is located in a river basin connected to marine receptor cell j . The impact of marine eutrophication finally occurs in the cLME subsegment associated with marine receptor cell j . Note that Fig. 2B only illustrates deposition in a single cell. This is a simplification, as emissions from one cell are actually deposited in all grid cells globally.

Equation 2 ($CF_{i,ss}^{air,c}$) links emissions to air with deposition and final environmental impacts in coastal water subsegments drawing on the method of Bjørn et al. (2020b). This CF is composed of one direct (first term of Eq. 2) and two indirect

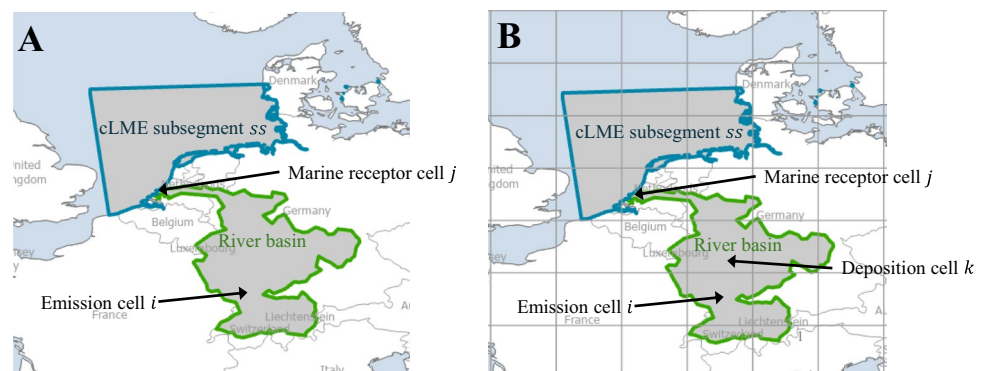
pathways (second and third term of Eq. 2), where the direct pathway involves nitrogen depositing directly on coastal or ocean water, whereas indirect pathways involve nitrogen depositing on another surface (i.e., soil or freshwater) and undergoing additional fate processes before reaching the coast:

$$CF_{i,ss}^{air,c} = \sum_{k \in ss} FE_{i,k}^{air,c} \times F_{k,ss}^{ocean} \times T_k \times XF_{ss} + \sum_{k \in ss} FE_{i,k}^{air,c} \times F_{k,ss}^{fw} \times FE_{k,j}^{fw} \times T \times XF_{ss} + \sum_{k \in ss} FE_{i,k}^{air,c} \times (1 - FPU_k) \times F_{k,ss}^{soil} \times FE_{k,j}^{soil} \times T_j \times XF_{ss} \quad (2)$$

Where:

- $CF_{i,ss}^{air,c} \left(\frac{kgO_2}{kgN_j/year} \right)$ translates the emission of the reactive nitrogen compound c (NO_x or NH_x) to air in cell i to decrease in oxygen levels in the benthic zone of subsegment ss .
- $FE_{i,k}^{air,c} \left(\frac{kgN_j}{kgN_i} \right)$ is the fraction of the emissions of reactive nitrogen compound c to air in cell i exported to the intermediate deposition cell k .
- $F_{k,ss}^{ocean} [-]$ is the surface area fraction within deposition grid cell k covered by ocean (including coastal and open ocean) with coastal residence time in subsegment ss .
- $F_{k,ss}^{fw} [-]$ and $F_{k,ss}^{soil} [-]$ are surface area fractions within deposition cell k covered by freshwater or soil respectively, within a river basin discharging to subsegment ss .
- $FE_{k,j}^{soil} \left(\frac{kgN_j}{kgN_i} \right)$ and $FE_{k,j}^{fw} \left(\frac{kgN_j}{kgN_i} \right)$ are fractions of depositions to soil or freshwater onto deposition cell k to marine receptor cell j .
- T_k and $T_j \left(\frac{kgN_j}{kgN_j/year} \right)$ are residence times in the coastal water of nitrogen transported to ocean deposition cell k or marine receptor cell j .
- $XF_{ss} \left(\frac{kgO_2}{kgN_{ss}} \right)$ is the exposure factor, i.e., the oxygen decrease in the benthic zone in response to the presence of nitrogen in coastal waters in the marine subsegment ss associated with the marine receptor cell j or k .

Fig. 2 **A** Spatial link between an emission to soil or freshwater in cell i , marine receptor cell j (river mouth) and its associated marine eutrophication impact in a cLME subsegment. **B** Spatial link between an emission to air in cell i , deposition in cell k , marine receptor cell j (river mouth), and its associated marine eutrophication impact in a cLME subsegment



- FPU_k is the fraction of plant uptake of nitrogen depositing in cell k considering nitrogen taken out of the impact pathway through crop harvesting or livestock grazing.

Note that for the direct pathway (first term of Eq. 3), depositions on both coastal waters and open ocean and their subsequent impacts in coastal areas are considered. However, nitrogen deposition on the open ocean will typically have very low coastal residence times, reflecting that only a small share of nitrogen deposition on the open ocean will be transported to the coastal domain and spend time here.

Equation 3 ($CF_i^{air,c}$) accumulates the CFs for all receiving coastal subsegments (ss) into a set of CFs for each emission cell (i):

$$CF_i^{air,c} = \sum_{ss} CF_{i,ss}^{air,c} \quad (3)$$

2.1.2 Model components and refinements

A summary of parameters, sources, substance flows, compartments, resolution, and main refinements associated with each method component compared to previous studies is presented in Table 1.

Inland fate component We adapted the work of Jwaideh et al. (2022) to create inland FEs (fractions exported from soil and freshwater). Jwaideh et al. (2022) used the Integrated Model to Assess the Global Environment-Global Nutrient Model (IMAGE-GNM) (Beusen et al. 2015) to develop a new spatially explicit FF model representing the fate and transport of nutrient emissions to and in coastal waters. Rather than directly using these FFs of Jwaideh et al. (2022), in our study, we extracted and adapted the underlying FEs. We did this as the original FFs encompassed erosion and leaching of background nitrogen compounds. In regions with steep terrain (e.g., Norway, Chile, the Alps, and Northern Spain), the FEs derived in Jwaideh et al. (2022) exceeded 1 (some even up to 6), implying more nitrogen was exported than introduced to the soil due to natural nitrogen’s erosion and leaching. In this study, we are interested in the impacts that can be attributed to human-caused emissions. Hence, we adapted the original FEs to account exclusively for new nitrogen added to the soil by dividing the original FEs by the historical fertilizer transient state fraction used in Jwaideh et al. (2022) to account for historical nitrogen inputs.

Table 1 Summary of characterization factor components and SOS, including their parameters, source, substance flows, resolutions, and main refinements necessary for the model coupling of this study

Component	Parameters	Source	Substance flow	Resolution	Refinements in this study
Inland fate (soil and freshwater)	FE^{fw} FE^{soil}	(Jwaideh et al. 2022)	DIN	5 arcmin (0.083°)	-Global coverage -Excluding export of background/inherent N -Coupling between FE and marine components based on PCR GLOBWB 2 (Sutanudjaja et al. 2018) -Determination of terminal basins
Air fate	FE^{air} FPU F^b	(Roy et al. 2012), (Schulte-Uebbing et al. 2022a, b)	NH_x, NO_x	2° × 2.5°	-Global coverage -Including impacts of deposition in the open ocean -Including plant uptake -Including denitrification
Marine fate	T	(Vea et al. 2022)	N	1/8° ^a	-Global coverage -Coastal residence time (CRT) at its original resolution (1/8°), using CRT at the river mouth and not average CRT over subsegment ^d
Exposure	XF	(Vea et al. 2022)		cLME subsegment	-Global coverage
Safe operating space	SOS	(Vea et al. 2022)		cLME subsegment	-Global coverage

^aCRT and PCR GLOBWB 2 river mouth location maps do not completely overlap, and there are missing CRT datapoints for some fjords or deep bays. Therefore, a buffer of using the average CRT within 25, 50, 75, or 100 km distance from the river mouth location in combination with a criterion of a minimum of 5 CRT data points was set. River mouths that did not meet these conditions were assigned a CRT value according to their closest neighbor

^bArea fractions of soil freshwater or ocean calculated using the intersection function in ArcGIS Pro v.2.6.2 (ERSI 2020) on shape files representing deposition grid cells (Bey et al. 2001), freshwater (rivers (Lehner and Döll 2004) and lakes (Messenger et al. 2016)), and ocean cover (Natural Earth 2023)

We linked inland grid cells to the coastal compartment, using river basins and their respective river mouths based on the hydrological model PCR GLOBWB-2 (Sutanudjaja et al. 2018). The original FFs (Jwaideh et al. 2022) had a resolution of 5 arcmin, but the river basin delineation relied on an older version of the model (PCR GLOBWB-1) with a 30-arcmin resolution. This created issues when connecting inland grid cells to river mouths, resulting in 187 instances where no connection could be established due to map misalignment, especially near the North Pole. In this study, we utilized PCR GLOBWB-2 to resolve these issues, while also providing other modeling enhancements, such as improved basin shape delineation and drainage network characterization (Sutanudjaja et al. 2018).

To identify terminal basins (water bodies not flowing into oceans), we also relied on PCR GLOBWB 2. Groundwater and evaporation flows are not considered in terminal basin classification (Wang et al. 2018) and are not considered in the PCR GLOBWB 2 model. Wang et al. (2018) emphasize substantial water storage changes in terminal basins, with groundwater discharge being a significant flux (possibly around 80% of net endorheic water loss). To consider uncertainties in the PCR GLOBWB 2 model and potential export to the ocean via groundwater flows, we assumed that a portion of nitrogen lost to groundwater in basins with a river mouth located less than 100 km from the coast is exported to coastal regions. This assumption and 100-km buffer are consistent with assumptions in IMAGE-GNM.

Air fate component For air emissions and their associated FEs, we employed the environmental fate model and associated source-receptor matrices of Roy et al. (2012). These matrices quantify the fraction (dimensionless) of air emissions (NO_x or NH_3) deposited on any spatial unit in a $2^\circ \times 2.5^\circ$ grid (13,104 grid cells). This renders 13,104 source-receptor matrices, each representing the deposition from one emission cell in the $2^\circ \times 2.5^\circ$ grid resolution.

While past studies considered the impact of the nitrogen deposition directly on the coastal domain and the indirect impact from nitrogen depositing on land and later transported to coastal areas (Bjørn et al. 2020b), we extended our method to include nitrogen deposition on the open ocean and its subsequent impact in the coastal zone. The CRT model of Liu et al. (2019) estimates the time a water parcel in the coastal zone or open ocean spends in any part of the coastal domain. Hence, the nature of the model and CRT parameter allowed us to include nitrogen deposition on the open ocean, by connecting atmospheric deposition grid cells with the CRT for open ocean water parcels from Liu et al. (2019). However, information about the specific transportation path and in which coastal subsegment a water parcel spends time is not explicitly given by the model. Therefore, we approximated

that the water parcel in a specific ocean grid cell will be present in the part of the coastal domain closest to the ocean grid cell. Based on this approximation, we attributed values to the XF and SOS components according to the values of the subsegment closest to the ocean deposition grid cells.

In Bjørn et al. (2020b), denitrification and uptake by vegetation were disregarded in the air emission impact pathway as the underlying NEWS-2 model considers the boundary between the technosphere (the anthroposphere) and ecosphere (the biosphere) at the point where nitrogen is leaching from the soil in the agricultural field. This means that all nitrogen deposited on soil was assumed to enter into the environment through surface runoff or leaching (i.e., disregarding removal by denitrification and plant uptake), and hence, the impact from nitrogen emissions was overestimated (Bjørn et al. 2020b).

In contrast, our study coupled soil deposition with IMAGE-GNM-based FEs, defining the technosphere-ecosphere boundary where nitrogen is available for leaching after plant uptake, volatilization, and nitrification. Therefore, denitrification in the air emission pathway was included in our CFs. In addition, we considered nitrogen removed through crop harvesting or livestock grazing by incorporating the fraction of plant uptake (FPU) parameter (refer to Fig. 1). This was an area-weighted average of the plant uptake fractions on arable and intensively and extensively managed grassland, calculated from Schulte-Uebbing et al. (2022a, b) data. FPU indicates the proportion of nitrogen taken up by plants relative to total nitrogen inputs, accounting for fertilizer, manure, fixation, and deposition. Our underlying assumption is that nitrogen deposited on arable and managed grassland and taken up by vegetation is removed through harvesting and grazing, while nitrogen deposited on natural land remains within the system and impacts pathway.

Marine fate component For the marine fate component (T), we adapted the Veia et al. (2022) approach, which relies on coastal residence times (CRT) from Liu et al. (2019). CRT represents the time a parcel of water is spending in the coastal domain (defined by the 200-m isobath) before it exits to the open ocean. Veia et al. (2022) aggregated the T into 289 cLME subsegments, approximating the geographical scale of eutrophication and hypoxia. Nevertheless, T at a specific site (e.g., river mouth) might not be representative of other locations along the shelf, as noted by Liu et al. (2019).

In our study, we calculated T by averaging areas closer to the original CRT resolution ($1/8^\circ$), encompassing spatial variability within each subsegment. For connecting PCR GLOBWB-2 river mouths with T , we employed the spatial join function in ArcGIS Pro v.2.6.2 (ERSI 2020). However, CRT and PCR GLOBWB-2 river mouth location

maps did not fully align, resulting in some missing CRT data points for fjords or deep bays. This is because the original CRT map's non-uniform tripolar grid, which distorts into two poles in the north while being regular in the southern hemisphere. We re-gridded the CRT tripolar grid to a uniform regular grid by the help of the `geoloc2grid` function in Matlab. However, there were still some issues with projecting this CRT map close to the North Pole. To address this mapping discrepancy and potential river mouth location inaccuracies, we introduced a buffer while joining the maps. We utilized the average CRT within 25, 50, 75, or 100 km from the river mouth, combined with a minimum CRT data point criterion. River mouths not meeting these conditions received a CRT value based on the nearest neighbor.

Global coverage To achieve global coverage including areas omitted by earlier marine eutrophication LCIA methods limited to LMEs, we re-ran the model of Jwaideh et al. (2022), computing FEs for previously excluded inland grid cells. Marine fate components (T) for these areas were calculated based on the raw CRT data from Liu et al. (2019) as previously mentioned. Global coverage is defined as covering all ice-free continents globally; i.e., Greenland and Antarctica and remote islands such as Hawaii are not included.

The marine area not yet included in any LCIA methods was segmented by limiting it to the coastal part (200 m isobath) and dividing the coastal part into subsegments with an area similar to the global average area extent of marine eutrophication (refer to Veia et al. (2022) for further details). By applying this approach, we complemented the existing 289 subsegments from Veia et al. (2022) with 16 new coastal subsegments, yielding a comprehensive 305 subsegments covering the global coastline. XFs, SOS, and pertinent parameters for these new subsegments were computed following the procedure described in Veia et al. (2022). Please refer to Supplementary Information (SI)-1, Fig. S1 for an overview of the additional subsegments and SI-3, Table S1 for their corresponding XF and SOS data.

2.2 Sustainability assessment and method comparison

To demonstrate the use of the method and to compare it with existing models, we apply it on a sustainability assessment case study. For the method comparison, we contrast our approach with that of Bjørn et al. (2020b), which is the only existing method that encompasses emissions to all compartments (soil, freshwater, coast, and air) and compares environmental impacts with SOS.

Our case study centers on open-field tomato production destined for processing (e.g., tomato sauce and paste). In order

to best demonstrate the large spatial resolution and global coverage of our method, we selected this case study because it has a large coverage (covers 197 farms distributed across nine countries and five continents) and has a high spatial specificity (with specific GIS-coordinates). Moreover, open-field tomato production emits nitrogen to both soil and air, hence enabling a demonstration of both the inland and air emission pathways of the method. Taking a focus on spatial differentiation, we exclusively account for direct emissions of nitrogen compounds from these farms, omitting emissions stemming from the production of fuels and agrochemicals used in tomato cultivation. For each of the 197 farms, we covered nitrogen oxides (NO_x) and ammonia (NH_3) emissions to air and nitrate (NO_3^-) to soil from fertilizer application, as well as NO_x emissions from the operation of agricultural machinery. Our reference flow is 1 t of tomatoes at the farm gate. Data sources are primarily drawn from Bjørn et al. (2020b), with some adaptations. Specifically, we excluded two farms from New Zealand due to imprecise coordinates locating them in the ocean. Furthermore, our model diverges from Bjørn et al. (2020a, b, c) in the interface between the ecosphere and technosphere. Bjørn et al. (2020b) considered the agricultural field as part of the technosphere and calculated nitrogen leaching from the agricultural soil in the inventory part. In contrast, our study encompassed leaching within the ecosphere and our CFs (see Sect. 2.1.2). To prevent double counting, we omitted leaching calculations in the inventory.

The environmental impacts ($\text{EI}(\text{kgO}_2)$) in cell j due to a nitrogen emission from a farm in cell i were calculated according to Eq. 4:

$$\text{EI}_{i,j}^m = M_i^m \times \text{CF}_{i,j}^m \quad (4)$$

where M_i^m (kg N/year) represents the total nitrogen emissions to compartment m in cell i and $\text{CF}_{i,j}^m$ (kg O_2 /kg N/year) the characterization factor for calculating its impact in cell j (as described in Eqs. (1) and (2)).

Finally, the environmental impact was compared to the SOS, to assess the occupation of the SOS according to Eq. 5:

$$\text{occ.SOS}_{i,j}^m = \frac{\text{EI}_{i,j}^m}{\text{SOS}_j} \quad (5)$$

where the SOS_j (kg O_2) is the safe operating space representing the difference between a boundary for minimum O_2 levels and natural reference level of O_2 in the coastal subsegment where receptor cell j is located.

Normally, to do an absolute sustainability assessment of a product or system, the SOS has to be assigned to the functional unit of the study. However, for simplicity, we did not assign SOS in this demonstrative case study, as the focus is on demonstrating the application of the new CFs of this study and comparing them to CFs from existing LCIA methods.

3 Results and discussion

3.1 Method results

3.1.1 CFs for soil emissions

Figure 3 shows global coverage CFs for emissions to arable soil, representing the estimated marine eutrophication impact (reduced O₂ concentration) for an emission of a nitrogen compound to soil. Refer to SI-1 Figs. S2–S3 for SOS and CFs encompassing emissions to all soils (weighted average of arable, grassland, and natural land CFs) and freshwater respectively.

Low CFs (green and light green in Fig. 3) are typically inland, while high CFs (orange and red in Figure) are closer to the ocean. This trend is due to reduced export of nitrogen compounds to the ocean from inland areas far from the shore, owing to removal processes during transportation (e.g., denitrification, nutrient uptake, and advection). Exceptions exist, such as low CFs near coasts like the northern Brazil

coast, Ivory Coast, and west India coast. For instance, grid cell #4,935,175 on the northern Brazil coast (highlighted in Fig. 3a) displays low CFs (7.00×10^{-8} versus global median of 1.06×10^{-2}) due to relatively low FEs (i.e., fractions exported) (6.84×10^{-5} versus global median of 1.71×10^{-2}). This can be explained by human obstructions such as dams causing low hydraulic loads. Furthermore, the marine fate component (T) is relatively low here (6.62×10^{-4} versus global median of 0.16) due to short coastal residence times. XF is also below the median (1.63 versus global median of 6.70) due to lower primary production potential.

The highest CFs are observed, e.g., near the coast of Gulf of Mexico, the Baltic Sea, and East China and Yellow Sea. In grid cell #3,269,522 (East China Sea, Fig. 2c), the CF is notably elevated (3.77 vs. global median of 1.06×10^{-2}) due to a high FE (0.74 versus global median of 1.71×10^{-2}). By comparison, the T and XF are close to the global median in that location, with T at 0.38 (vs. global median of 0.16) and XF at 10.02 (vs. global median of 6.70).

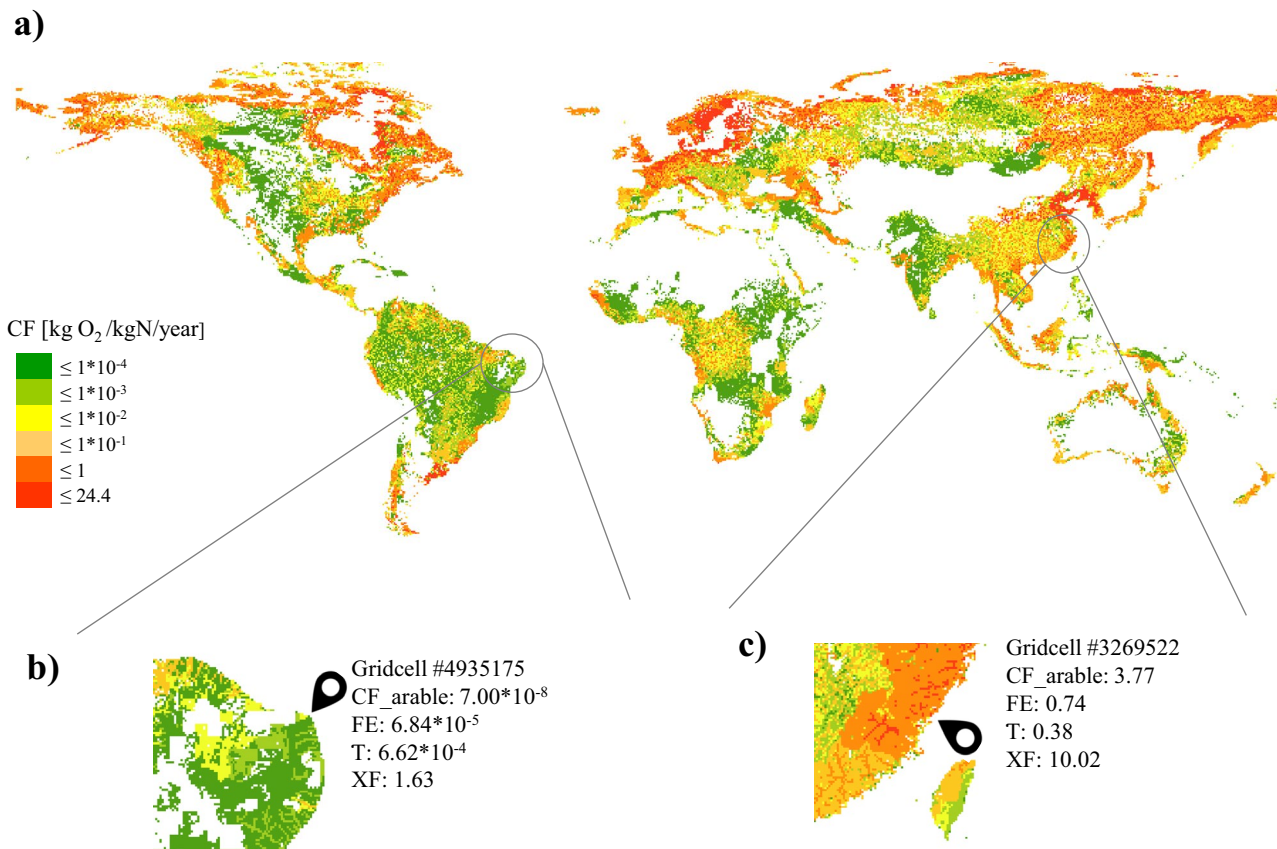


Fig. 3 a CFs (kg O₂/kg N/year) for emissions to arable soils representing the estimated marine eutrophication impact (reduced O₂ concentration) of a nitrogen emission to soil. **b** Zoom on grid cell 1,237,786 and information on associated CF components (i.e., inland

fractions exported (FE), marine fate component (T), and exposure factor (XF)). **c** Zoom on grid cell 4,935,175 and information on associated CF components

3.1.2 CFs for air emissions

In Fig. 4a, CFs for NO_x are shown in each emission cell, representing the cumulative CFs for associated deposition cells (as calculated by Eq. 4). For example, the cell highlighted with a blue star in Fig. 4a (near Hudson Bay in North America) displays a higher-end CF (orange color) because large shares of emissions from this cell deposit onto cells with high partial CFs (pCFs). The pCF translates nitrogen deposition on soil, freshwater, or ocean to impacts by considering nitrogen transport and subsequent coastal fate and exposure. Figure 4b illustrates this, depicting deposition shares (size of beige circles) in cells receiving >0.1% of NO_x emissions from the cell highlighted with a blue star along with pCF values in each deposition cell. Notably, deposition shares are highest in cells close to the emission cell where the pCFs are also large (red color). Large pCFs in these deposition cells are primarily due to high coastal residence times and absence of plant uptake removal in cells without agricultural land.

In contrast, the cell highlighted with a black star in Fig. 4a and c (south of India) exhibits lower-end CFs due to low pCFs in deposition cells receiving significant shares of nitrogen emissions from this source (green and yellow color in Fig. 4c).

Low pCFs in these deposition cells result from short coastal residence times and high plant uptake in cells containing agricultural land.

Note that air emission CFs represent impact per kg NO_x-N or NH_x-N. To convert inventory emissions (e.g., 1 kg NO₂ emitted to air) to nitrogen mass in the NO₂ form, a stoichiometric conversion (by multiplying with 0.304) is needed. Similarly, for emissions to soil and water, CFs reflect potential impact of 1 kg reactive nitrogen. Hence, if the emission is reported as, e.g., kg NO₃⁻ in the inventory, a stoichiometric conversion is needed by multiplying the NO₃⁻ emissions of the inventory by 0.226.

3.2 Case study and comparison to similar method

3.2.1 Occupation of safe operating space of nitrogen emissions from tomato production

In Fig. 5a, each of the 197 tomato production farms' locations and coastal occupation of SOS (occ.SOS) resulting from nitrogen emissions from all farms to soil and air are depicted (blue pins). The largest occ.SOS is found in sub-segments receiving emissions from soil (indicated by black

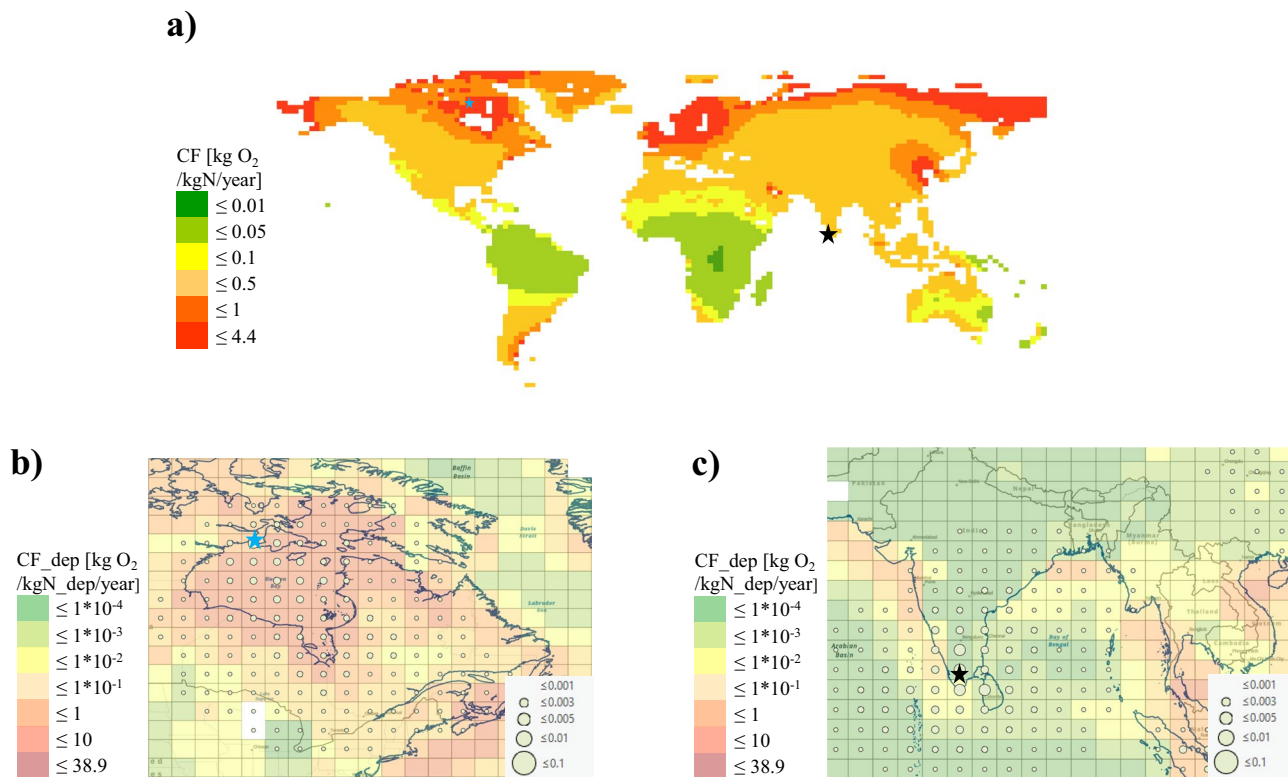


Fig. 4 a Map showing the NO_x CFs (kg O₂/kg N/year) in each emission cell, i.e., cumulative CFs for deposition cells associated with each emission cell. Maps of North America (b) and India (c) show deposition shares in cells receiving >0.1% of NO_x emissions from cells marked with a blue and black star, respectively. The size of

deposition shares is indicated by the size of the beige circles (10 to 0.1%). Color scales in maps b and c show partial CFs's values for nitrogen deposition in each grid cell (kg O₂/kg N_{dep}). Refer to SI-1, Fig. S4 for CFs for emissions of NH_x to air and to SI-3–Supplementary Data for data underlying this figure

lines in Fig. 5b–d); particularly in subsegments #42.1 and #25, the occ.SOS is large (2.6×10^{-5} and 7.2×10^{-6} respectively). This substantial occ.SOS stems primarily from large amounts of nitrate emissions to soil and nitrogen export (i.e., FEs). However, in some subsegments that receive emissions from soil, the occ.SOS is low. For example, subsegment #34.1 has a low occ.SOS with a value of 1.3×10^{-9} (Fig. 5c). This is attributed to minimal environmental impact resulting from low emissions from the nearby farms and low fractions exported (FE). Figure 5c illustrates the spatial relationship between locations of farms and coastal segments where nitrogen is exported (thick gray line outlining river basin areas containing farms that drain into subsegments #34.1). As explained in Sect. 3.2.2, greater travel distance from the point of emission to coastal segment generally leads to lower nitrogen export fractions to the ocean, owing to removal processes during transportation.

As shown in Fig. 5a, all coastal subsegments receive nitrogen due to air emissions from the tomato farms

transported and depositing all over the globe. Nonetheless, occ.SOS remains quite low in most coastal subsegments (196 of 305 subsegments have an occ.SOS below 1×10^{-8}) due to the widespread dilution of the air emissions. In specific cases, larger occ.SOS driven by air emissions is noted, such as in subsegments #24.4 and #22.6 (Fig. 5c) with an occ.SOS of 2.8×10^{-7} and 5.0×10^{-7} , respectively, caused by air emissions from the opposite side of the continent (i.e., in Spain and Portugal about 1500–1900 km away). The larger occ.SOS is due to relatively large nitrogen emissions from these farms (20 t compared to 76 t from all farms) and that a relatively large share deposits directly on these coastal subsegments where the marine fate component is high. For example, about 2% of the nitrogen emissions from the farms located in Spain and Portugal deposit on subsegment #22.6, compared to 0.03% if emissions were distributed equally across all grid cells. Globally, the accumulated total environmental impact of air emissions from the 197 farms leads to a similar level of impact as caused by soil emissions (1.2×10^4

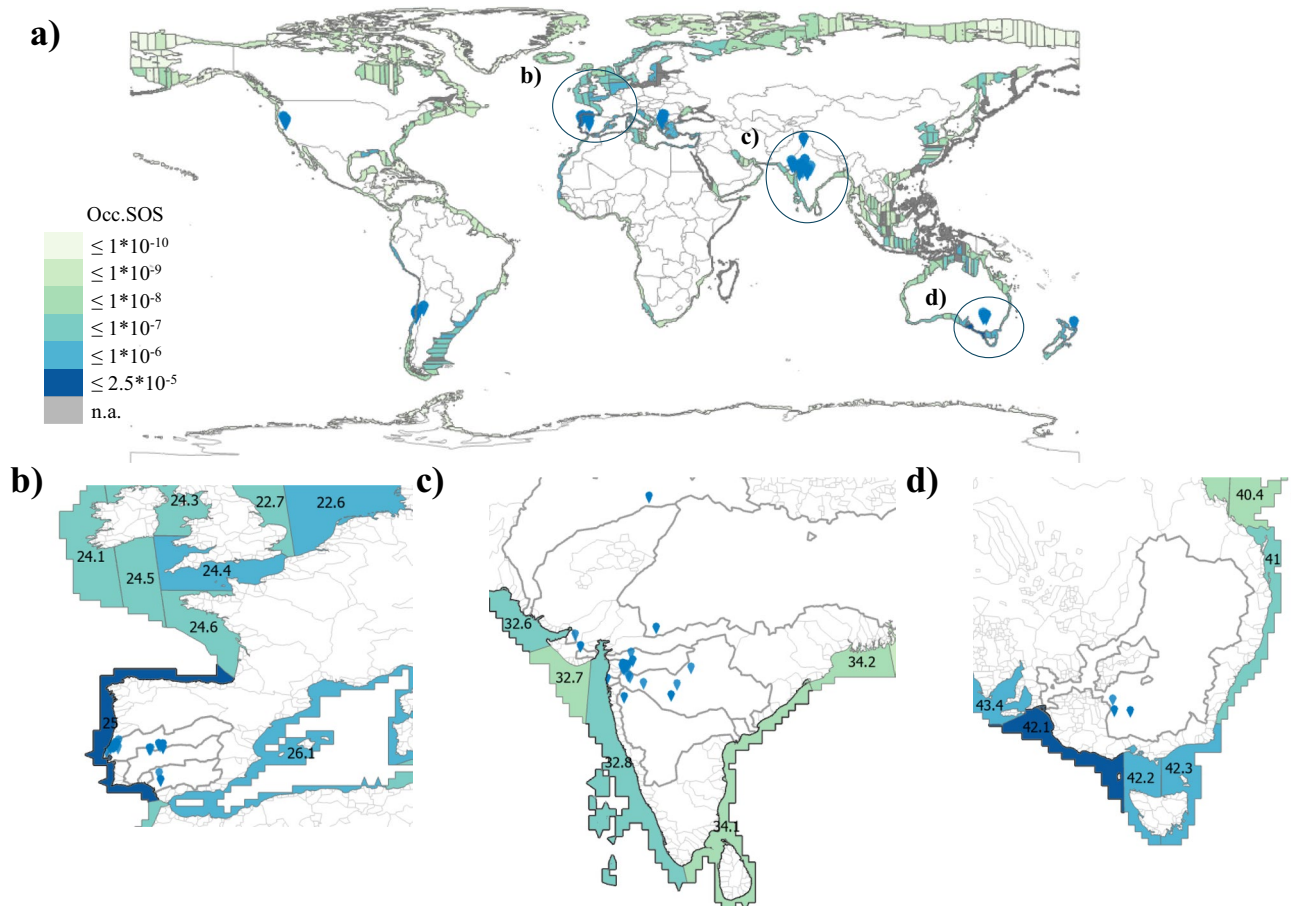


Fig. 5 occ.SOS resulting from nitrogen emissions to soil and air from the 197 tomato production farms, accumulated into relevant coastal subsegments. The farms are located in six different regions of the world (pins in Fig. 5a). **b–d** Maps showing selected zooms where the

thick gray delineations illustrate the river basins in which the farms are located in and their connection to the coastal subsegments and the thick black lines indicate coastal subsegments that are directly connected with the river basins receiving nitrogen from soil emissions

kg O₂, compared to 3.0*10⁴ kg O₂, respectively). However, due to the widespread global transportation of the air emissions, they contribute less than soil emissions to coastal sub-segments' occ.SOS (subsegments receiving soil emissions are marked with a thick black line in Fig. 5b–d).

3.2.2 Comparison of the method developed here to a reference method

Soil emissions Table 2 presents nitrate emissions from the case study farms to soil and their associated environmental impacts, SOS, and occ.SOS using our method (Table 2a) and the method of Bjørn et al. (2020b) (Table 2b). The color shades from green, yellow to red indicate increasing emissions, impact, SOS, or occ.SOS.

The first columns of Table 2a and b display the amount of nitrate emissions to soil in river basins or watersheds discharging to the different coastal segments, using our method and the method of Bjørn et al. (2020b), respectively. Our study generally reports higher emissions (1.4–3.3 times), due to different soil CFs' inventory input calculation detailed in Sect. 2.1.2. In our study, we consider nitrogen from fertilizer and manure,

adjusted for plant uptake, volatilization, and nitrification (NH₃ and NO_x). In Bjørn et al. (2020b), the inventory input comprises NO₃⁻ leaching, calculated by an empirical model. This approach disregards the actual nitrogen remaining for potential leaching after other loss mechanisms. Consequently, 47 out of 199 farms in Bjørn et al. (2020b) demonstrated a negative nitrogen inventory mass balance (inputs-outputs < 0). By integrating leaching into the ecosphere and CF model (as in this study), we address this issue of negative mass balance resulting from using individual models to calculate the different parts of the nitrogen cycle in the inventory. Regarding ranking of emission quantities, there is a general agreement between this study and that of Bjørn et al. (2020b). For example, farms in river basins discharging to cLMess 25 and LME 25 have the highest emissions, while those discharging to cLMess 26.3 and LME 26 have the lowest emissions.

In the second columns of Table 2a and b, we observe differences in EI between our study and Bjørn et al. (2020b). In our study, EI is higher in three cases (subsegments #13.3, 25, and 42.1), while Bjørn et al. (2020b) reports higher EI in five cases (subsegments #26.3, 26.4, 32.6, 32.8, and 34.). The overall ranking of EI across the ten coastal segments is similar in both studies, with three exceptions. Subsegment

Table 2 Amount of nitrate emissions to soil, environmental impact (EI), safe operating space (SOS) and occupation of SOS (Occ.SOS) from the 197 farms, accumulated into relevant subsegments or LMEs

calculated by the method presented in this study and by the method of Bjørn et al. (2020b), respectively. Color shades from green, yellow to red, indicate increasing values.

a) This study					b) Bjørn et al., 2020b				
Sub-segment	Emissions (kg N/year)	EI (kg O ₂)	SOS (kg O ₂)	Occ.SOS	LME	Emissions (kg N/year)	EI (kg O ₂)	SOS (kg O ₂)	Occ.SOS
3 ^a	0	0	4.2E+09	0	3	3.2E+03	2.9E+02	1.1E+11	2.6E-09
13.3	3.5E+04	1.5E+03	6.6E+09	2.2E-07	13	1.9E+04	4.4E+02	1.2E+11	3.7E-09
14.10 ^b	2.9E+03	0	4.3E+09	0	14	2.0E+03	4.5E+01	4.2E+10	1.1E-09
25	2.2E+05	7.2E+03	1.0E+09	7.0E-06	25	1.4E+05	5.6E+03	1.2E+10	4.6E-07
26.3	6.6E+02	1.0E+01	2.1E+09	4.7E-09	26 ^c	2.5E+02	2.2E+02	1.0E+11	2.2E-09
26.4 ^c	9.0E+03	8.9E+02	1.9E+09	4.7E-07	26 ^c	3.4E+03	3.1E+03	1.0E+11	3.0E-08
32.6	6.2E+03	3.6E-04	2.4E+09	1.5E-13	32 ^c	4.5E+03	4.8E+02	2.4E+11	1.9E-09
32.8 ^d	1.3E+03	4.9E+01	3.4E+09	1.7E-08	32 ^c	9.3E+02	7.4E+01	2.4E+11	3.0E-10
34.1	1.5E+03	2.4E-03	2.3E+09	1.1E-12	34	9.1E+02	4.4E+02	2.1E+11	2.1E-09
42.1	1.5E+05	2.1E+04	8.2E+08	2.5E-05	42	4.6E+04	1.1E+02	6.2E+10	1.7E-09

^aThere are no NO₃⁻ emissions (leaching) from the farms located in grid cells exporting to subsegment #3 in this study according to the inventory calculations required by our method

^bThere is no export of nitrogen from the grid cells where the farms located in the river basin discharging to subsegment #14.10 are located

^cOur method did not consider impacts of emission from three farms exporting to subsegment 26.4 because the resolution in this study fails to include and provide CFs for some parts of the land area very close to the ocean

^dOur method considers no export from the grid cells where four farms exporting to subsegment #32.8 are located

^eFor comparison, the results of Bjørn et al. 2020b for LME 26 and 42 were divided into subsegments according to the portion of environmental flows exported to the subsegments calculated by our method

#42.1 has the highest EI in our study but ranks among the lowest in Bjørn et al. (2020b). Conversely, subsegments #32.6 and 34.1 have low EI in our study but high EI in LME 34 according to Bjørn et al. (2020b). The differences in EI and their ranking can be attributed to the spatial resolution of our study, which uses finer spatial grids for fractions exported (FE) and marine fate components (T) compared to Bjørn et al. (2020b), who use watershed-level FEs and LME-level T . In cases with significant spatial variability, this difference in resolution can lead to vastly different EI estimations. For example, the EI estimated in LME 34 is five orders of magnitude higher in Bjørn et al. (2020b) compared to our study. The FEs in grid cells discharging to LME 34 vary greatly between the two studies, with Bjørn et al. ranging from 1.4×10^{-1} to 3.8×10^{-3} , while ours spans from 6.7×10^{-5} to 9.6×10^{-19} . As discussed in Sect. 3.2.1, low FE in our study is due to their location far west in the river basin exporting to subsegment #34.1. In contrast, Bjørn et al. (2020b) employ watershed-level FE and, consequently, overlook these differences within the watershed. The marine fate component (T) in segment 34 also differs significantly, with Bjørn et al. (2020b) estimating 1.74 years, while our study calculates values of 0.004, 0.039, 0.535, and 0.547 depending on to which river mouth to which the nitrogen is transported. In addition to being associated with a high level of uncertainty (discussed in Veá et al. (2022)), the T estimates in Bjørn et al. (2020b) do not consider such spatial differences in residence time within the LME. It is important to note that the T values derived in this study are not directly comparable to Bjørn et al. (2020b) as they denote the duration a nitrogen load stays in the coastal part of an LME segment in our study, as opposed to the entire LME segment. Hence, larger values are expected in Bjørn et al. (2020b).

Column three of Table 2a and b shows that the SOS is smaller in this study compared to Bjørn et al. (2020b) due to adjusted parameters and refined resolution of the marine compartment (for details, see Veá et al. (2022)). The overall ranking of SOS across the ten coastal segments is generally consistent between both studies, except for cLMEs 14.10, ranking as the second largest in this study and as the second lowest in Bjørn et al. (2020b). This discrepancy is linked to the relatively high O_2 reference value in our study ($9.2 \text{ kg } O_2/l$ compared to the average of $4.9 \text{ kg } O_2/l$ across the ten segments) compared to the one estimated in Bjørn et al. (2020b) ($9.5 \text{ kg } O_2/l$ compared to average of $8.3 \text{ kg } O_2/l$ across the ten segments).

As displayed in the fourth column of Table 2a and b, the occ.SOS calculated in our study is larger than Bjørn et al. (2020b) in six subsegments (#13.3, 25, 26.3, 26.4, 32.8, 42.1), primarily due to the smaller SOS. In two subsegments (#32.6, 34.1), the occ.SOS is higher in Bjørn et al. (2020b), provided by the larger EI in these subsegments explained above. Comparing rankings of occ.SOS across coastal areas reveals there is general

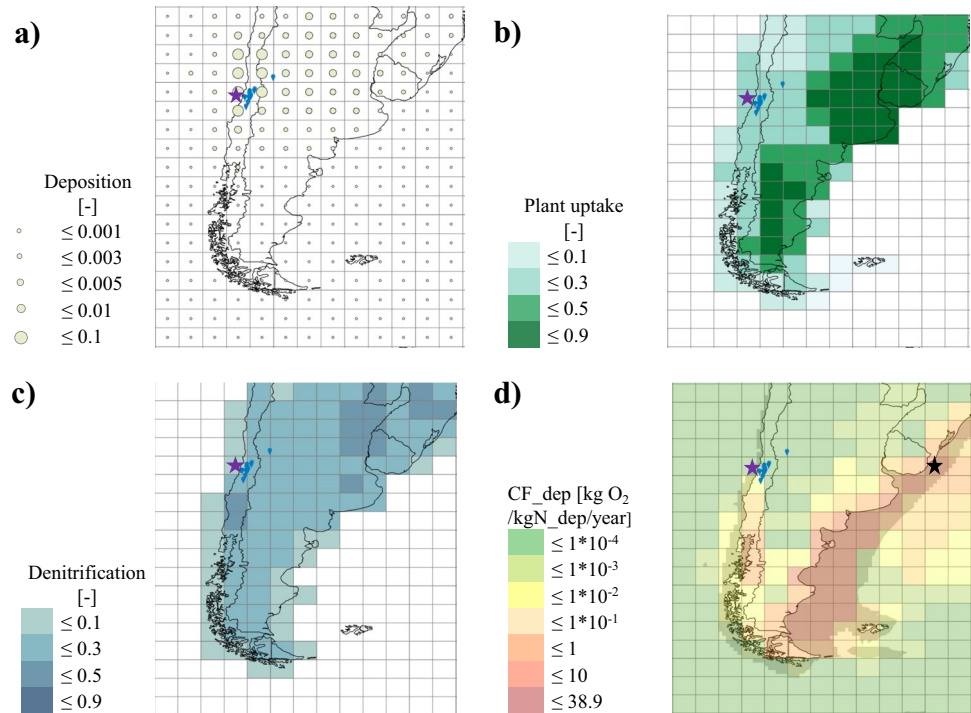
agreement when using our method and Bjørn et al. (2020b). However, while our study identifies subsegment #42.1 as having the highest occ.SOS, using Bjørn et al. (2020b) places LME 42 as the third lowest due to the low EI discussed above.

Air emissions Given the complexity of the air emission model (involving three different deposition pathways and 13,104 deposition cells for each emission cell), this comparison focuses on a single farming area. Moreover, a thorough comparison of the CF components (i.e., the FEs, T , and XFs) and SOS involved in the different deposition pathways was already conducted in the previous section. Therefore, this section focuses on the fundamental differences between our method and Bjørn et al. (2020b) specific to the air emission pathway, encompassing (1) plant uptake fraction, (2) denitrification, and (3) deposition on open ocean.

In Bjørn et al. (2020b), denitrification and vegetation uptake loss mechanisms were disregarded in the impact pathway for air emissions, as the authors considered the technosphere-ecosphere boundary at the point of leaching. This means that all nitrogen that deposits on soil was assumed to enter into the environment through surface runoff or leaching. Figure 6 shows a zoom on the area around grid cell 4076 in Chile (highlighted with a purple star), where ten farms are located emitting a total of 446.0 kg N-NO_x and 1945.8 kg N-NH_x per year causing a cumulative global reduction of $447 \text{ kg } O_2$, according to the method developed here. Figure 6a shows the portion of nitrogen deposition on each cell associated with the emission cell. Figure 6b-d shows the fraction of plant uptake, denitrification rate, and CFs associated with the receiving cells. Our method reveals that a cumulative 16.3% of nitrogen emitted by farms in grid cell 4076 is removed through plant uptake, and 10.1% is removed via denitrification upon soil deposition (summing removal amounts from each deposition cell in Fig. 6a and b). Incorporating these removal mechanisms reduces the total estimated impacts of emissions in grid cell 4076 by 34.2%. Hence, including these removal mechanisms in the emission pathway as done in this method is important to avoid substantial overestimation of impacts.

In contrast to the approach used by Bjørn et al. (2020b), we included open ocean nitrogen deposition beyond the LME marine area. Figure 6a shows that small portions of nitrogen emitted from grid cell 4076 deposits in the ocean outside the LME boundary (dark shade in Fig. 6d). However, in total, approximately 29.9% of nitrogen emitted in cell 4076 deposits in the ocean outside the LME borders, causing 5% of the associated impacts through subsequent transport to an LME. This emphasizes the need to include open ocean deposition to prevent underestimating impacts. In some emission cells, the impact contribution of nitrogen deposition on the open ocean is even more significant. For instance, if farms were situated

Fig. 6 Zoom on the area surrounding grid cell 4076 in Chile (highlighted with a purple star), where six of the case study farms are located. **a** The portion of nitrogen deposition on each cell associated with the emission cell. **b–d** The plant uptake fraction, denitrification rate, and CFs in the receiving deposition cells associated with the emission cell as estimated in our method. The black star in **d** indicates grid cell 4084 where the impact contribution of nitrogen deposition on the open ocean is large.



close to the coast of Uruguay (e.g., grid cell 4084 denoted by a black star in Fig. 6c), 43.8% of emitted nitrogen would deposit in the open ocean, contributing to 18.6% of the total impacts of emissions in this cell.

4 Uncertainties, limitations and future research

4.1 Method development

Our study coupled state-of-the-art nitrogen emission impact assessment models, for which sensitivity and uncertainty analysis, model validation, and discussion of limitations have been performed and documented in their original sources (refer to, e.g., Jwaideh et al. 2022; Roy et al. 2012; Veá et al. 2022 for details). Thus, a comprehensive parameter analysis and model validation fall outside the scope of this study. Instead, this section summarizes uncertainty and sensitivity assessments for the main method components and parameters found in the original method and model sources. By this, we will highlight priorities for future research to increase the accuracy of our method and to guide practitioners on how to interpret the results of our method.

4.1.1 Inland fate component

The inland fate component draws on work of Jwaideh et al. (2022) that used equations from the IMAGE-GNM model as a basis for their method. IMAGE-GNM was validated

with observations in Beusen et al. (2015) and more recently in Beusen et al. (2022) where they conclude that IMAGE-GNM shows a fair to good agreement with observations. Beusen et al. (2022) do not address the uncertainty of individual model parameters, but highlight parameters with a high influence on the model results, including total runoff, temperature, uptake velocity, and parameters used to estimate the in-stream retention, such as mean length of streams and length ratio (Beusen et al. 2022).

The inland fate component is based on simulations of conditions from the year 2000 (Jwaideh et al. 2022). Meanwhile, LCA and AESA generally aim to reflect yearly average conditions. Hence, we recommend future research to extend the datasets used within IMAGE-GNM to multiple years, to be able to assess inter-annual fluctuations in model parameters and the resulting characterization factors.

While the inland fate component contains a degree of uncertainty, it is based on a state-of-the-art model (IMAGE-GNM). Hence, our method reduces uncertainties related to, e.g., missing inland fate components in existing methods relying on NEWS 2. Moreover, we have shown that the high spatial resolution in our method reduces the uncertainty related to spatial variabilities.

4.1.2 Air fate component

The atmospheric fate component in our method was based on source-receptor matrices from Roy et al. (2012). A study applying the same source-receptor matrices (Roy et al. 2014) estimated the spread of the 95% confidence interval of the

probabilistic atmospheric FF to be 0.79–1.26. This uncertainty assessment was done through Monte Carlo simulations where the variation of each FF was specified with lognormal distribution following accuracy observations by Roy et al. (2012). Model uncertainties and uncertainties due to choices were addressed qualitatively in Roy et al. (2014), and it was highlighted that due to the coarse resolution ($2^\circ \times 2.5^\circ$), local factors favoring deposition in certain regions within the grid (e.g., mountains) are neglected. Philip et al. (2016) tested the sensitivity of different spatial resolutions in the source model (GEOS-Chem) and found that decreasing the spatial resolution from $2^\circ \times 2.5^\circ$ to $4^\circ \times 5^\circ$ altered the simulation results by an order of magnitude, indicating a high sensitivity to the spatial resolution.

Moreover, the source-receptor matrices are based on simulations using the GEOS-Chem model version 8–02–02 and meteorological data for the year 2005. While Roy et al. (2012) consider 2005 to be representative of the average conditions from 1961 to 1990, variations in meteorology between years could impact source-receptor relationships (Roy et al. 2012).

Updating these source-receptor matrices with data for additional years should be a focus of future methodological advancements. A way to achieve this is to generate updated matrices through new simulations using the latest GEOS-Chem model version and multiple meteorological reference years. Alternatively, exploring other global chemical transport models for deriving source-receptor matrices is possible, although their complexity often demands substantial computational and expert resources (Van Dingenen et al. 2018). Therefore, a viable option could be to use reduced-form source-receptor models like the TM5-FASST model, which computes atmospheric concentrations based on emission changes. Given its current reliance on a single reference year (2000) and regional aggregation, there are plans to develop an updated version based on more current reference simulations and meteorology (Van Dingenen et al. 2018). When available, its potential application in LCIA should be explored. Furthermore, the spatial resolution of the TM5-FASST model is at $1^\circ \times 1^\circ$; hence, the uncertainties related to the coarse spatial resolution of the GEOS-Chem model version 8–02–02 would also be reduced if applying the TM5-FASST model to compute new source-receptor matrices.

4.1.3 Marine fate component and SOS

For the marine fate component and estimation of SOS, Vea et al. (2022) showed that their method exhibited good agreement with empirical observations identifying critical areas where the SOS is exceeded. However, several parameters were found to be influential and associated with uncertainty. These parameters include O_2 reference level, O_2 critical level, and benthic zone depth for estimation of

SOS, XF, and CRT for marine fate and exposure estimation (refer to Vea et al. (2022) for details). In line with these findings, the method developed here builds on the best available data for these parameters and significantly reduces the uncertainty associated with previous methods (e.g., Bjørn et al. 2020b; Cosme and Hauschild 2017). For example, the CRT that drives the marine fate component was based on extrapolation from a few and highly uncertain data points (Cosme et al. 2018). In our method, we use high-resolution CRT derived from state-of-the-art global ocean-ice models. While these models contain a degree of uncertainty, in particular for inland seas, island chains, or heavily ice-covered systems, they are based on currently best available data from multiple models with global coverage and high resolution (Vea et al. 2022). Similarly, the most sensitive parameter in Vea et al. (2022) was the O_2 reference (representing an undisturbed environment) used for SOS calculation. While the O_2 reference relies on the average of simulations from six Earth system models, which all involve uncertainty, they nevertheless represent state of the art for Earth system modeling.

A crucial step in the development of the method of Vea et al. (2022) was the segmentation of the global coast based on global average area extent of eutrophication. This segmentation method does not account for spatial variations in the area extent of eutrophication, for example, caused by differences in transport mechanisms across regions. Future research could explore alternative segmentation approaches, e.g., estimating area extent of nitrogen transport from a point source. This would however require high-resolution data describing local effects such as transport flows and directions influencing freshwater plume structures, which is currently not available with global coverage for coastal segments (Vea et al. 2022). Moreover, to increase the accuracy, we recommend updating the sensitive parameters associated with a certain degree of uncertainty, when improved data becomes accessible.

4.2 Method application and operationalization

Our method and associated CFs may be applied in conventional LCA and in AESA (the latter along with associated SOS), under consideration of the limitations addressed above. This section will outline how our method can be applied for decision support and aspects to be aware of when doing so.

4.2.1 Decision support

Applying our method in a conventional LCA can provide information regarding the marine eutrophication impact of a studied system, enabling producers or suppliers to identify hot spots in their production or supply chain, or to compare with alternative products. This will allow for informed decisions

and targeted optimization in terms of reducing environmental impacts. In order to support damage modeling, our CFs can be combined with effect factors expressing impact results as ecosystem damage and loss of biodiversity. For this, the EFs developed in Cosme and Hauschild (2016) can be used. Moreover, our method could be combined with LCIA methods for other impact categories such as climate change, in order to avoid burden-shifting. For example, if assessing the impact of fertilizer applications, climate change impacts from denitrified nitrogen should also be considered.

Using our AESA method would add an extra layer to the decision support, namely, assessing whether the production that is assessed can be considered environmentally sustainable with respect to nitrogen emissions. If the production is assessed to be unsustainable, actors can consider whether altering their operations or product design could decrease their environmental impact to a level below the assigned SOS. In addition, the spatial differentiation of our method could provide decision support on where companies should source their materials. For example, our method could help identifying materials associated with nitrogen intensive farming operations that are produced in areas with low export to coastal segments and that has low occupation of the regional SOS.

At the national level for policy decisions, our AESA method may be used to assess how to sufficiently reduce environmental impacts of nitrogen emissions caused by a nation's consumption and production of goods and services that occur within and outside that nation. For this, our method could be coupled with multi-regional input output models allowing to analyze international trade patterns and their associated marine eutrophication impacts similar to Bidoglio et al. (2023), but also considering the SOS.

Globally, our method can contribute to understanding how to prevent exceeding nitrogen-related SOS in coastal waters, while allowing humanity to thrive. The planetary boundary concept (Richardson et al. 2023; Rockström et al. 2009; Steffen et al. 2015) has established SOS for Earth system processes essential for the functioning of the Earth system, including SOS for nitrogen emissions to the open environment. While regional variations were not initially accounted for, recent work related to the planetary boundaries by, e.g., Rockstrom et al. (2023), integrated spatial variations into Earth system boundaries, drawing from research of Schulte-Uebbing et al. (2022a, b). In their estimation of nitrogen boundaries, they considered thresholds related to (1) nitrogen deposition rates (to avoid or limit terrestrial biodiversity loss), (2) nitrogen concentrations in surface water (to limit eutrophication), and (3) nitrogen concentrations in groundwater (to meet the World Health Organization (WHO) drinking water standard). The critical nitrogen concentration in surface water was set with the objective

to protect coastal water. However, this critical concentration (Rockström et al. 2023; Schulte-Uebbing et al. 2022a, b) is spatially generic and does not account for the spatial variability in, e.g., coastal residence times and biological responses. These factors are important for the estimation of reduced oxygen concentration in bottom coastal waters driven by nitrogen inputs. To expand the scope of the nitrogen boundary, our method and associated CFs could be used to translate the spatially differentiated critical oxygen concentration limit to new nitrogen boundaries. Hence, this would render a boundary considering spatial variability in the whole impact pathway and with a better representation of the coast.

4.2.2 Delineation between ecosphere and technosphere

As discussed in Sects. 2.1.2 and 3.2.2, our method considers nitrogen leaching as a part of ecosphere (i.e., as a part of the CFs and LCIA), while the method of Bjørn et al. (2020b) considers the agricultural field (including leaching) as a part of the technosphere and LCI. However, to our knowledge, there is no consensus in the LCA community regarding the appropriate approach.

Similarly to the Glasgow consensus on the delineation between pesticide emission inventory and impact assessment for LCA (Rosenbaum et al. 2015), we propose that flexibility should be allowed when determining the boundary. This flexibility should correspond to the study's goal and scope, while also taking into account potential trade-offs. When LCA involves an agricultural background process, practitioners should verify that the inventory modeling matches the CFs to avoid double-counting leaching, either by adapting the background process or applying a set of CFs with the same delineation. For agricultural foreground processes, considering the field as a part of the LCI could be reasonable, especially if the goal of the study is to assess the effect of agricultural practices on leaching (e.g., catch crops or reduced tillage). However, as discussed in Section 2.1.2, considering leaching as a part of the ecosphere and CF model (as in this study) eases the data collection on the inventory part and mitigates potential negative mass balance resulting from using individual models to calculate the different parts of the nitrogen cycle in the inventory part.

To accommodate these different applications and needs, we provide a set of CFs where leaching is considered a part of the technosphere, along with the CFs where it is considered a part of the ecosphere (SI-1, Figs. S5 and SI-3 for CF data). However, to ensure consistency and avoid double counting, we propose launching an initiative akin to the Glasgow consensus, to establish consensus about the delineation between fertilizer emission inventory and impact assessment for LCA.

4.2.3 Aggregation and method operationalization

As demonstrated in the case study, our CFs apply to LCA studies with inventory data that can be spatialized to the resolution of our method. To extend their use to cases where the inventory cannot be spatialized to this degree, we suggest aggregating native resolution CFs into the relevant larger spatial scales (e.g., regional, national, continental, or global). Following UNEP-SETAC recommendations (Mutel et al. 2019), CFs should be aggregated using sector-specific emission weights. This minimizes errors from spatial variability when using large-scale aggregated CFs (Boulay et al. 2018). Such aggregation would also facilitate the implementation of the method in LCA software tools, as most of these are spatially restricted to country scales (Verones et al. 2020). The LCA software system Brightway (Mutel 2017) is however able to handle the fully spatially differentiated methods, and we recommend future studies applying our method to use such software if inventory data spatialized at a higher resolution than country scale is available.

For AESA, no guidelines currently exist on how to aggregate (1) spatially differentiated AESA method components (including SOS) when the exact location of an inventory flow is unknown (i.e., to match inventories with a coarser spatial resolution) and (2) the results of an AESA (occ.SOS) into one (or fewer) indicator that reduces complexity and is easier to communicate. In a case study involving activities with impacts on a large geographical scale (e.g., our case study where air emissions from tomato production impacted the entire global coast), the occ.SOS could be aggregated to ease the communication of the results. However, aggregating spatial AESA results presents challenges in maintaining information about potential local or regional exceedances (Bjørn et al. 2020c; Ryberg et al. 2018). Bjørn et al. (2020c) considered this issue and proposed to aggregate AESA results into “accumulated exceedances.” Future research should explore whether this accumulated exceedance is the best approach, or if there are alternative approaches, for example, considering existing aggregation approaches in the planetary boundary literature (e.g., Richardson et al. 2023; Rockström et al. 2023; Schulte-Uebbing et al. 2022a, b).

5 Conclusions

This study presents a complete LCIA method for calculating CFs that allow assessing the marine eutrophication impact of nitrogen emitted to any environmental compartment in relation to the relevant SOS, anywhere in the world. The method relies on models representing state of the art of their fields, and it addresses current limitations in existing marine eutrophication modeling in LCIA and AESA, such

as missing fate components in the inland nitrogen transport, poor data on fate in the coastal compartment, and a coarse spatial resolution. In the process of coupling the underlying models, we ensure global coverage by including hitherto missing coastal regions and integrating denitrification and plant uptake in the air emission pathway.

In the analyzed case study, we demonstrate that spatial variability within river basins greatly impacts the results, highlighting the significance of our method’s increased spatial resolution. Similarly, the finer resolution of coastal compartments results in larger occupations of SOS compared to existing methods. Despite remaining limitations, the method is considered robust as it is based on the best data and models currently available and significantly reduces uncertainty compared to existing methods. We strongly believe that our method can support more informed and better decisions for managing nitrogen and reduce emissions to sustainable levels.

Supplementary Information The online version contains supplementary material available at <https://doi.org/10.1007/s11367-024-02311-z>.

Funding Open access funding provided by Technical University of Denmark

Data availability The authors declare that the data supporting the findings of this study are available within the paper and its Supplementary Information files. Should any raw data files be needed in another format, they are available from the corresponding author upon reasonable request.

Declarations

Competing interests The authors declare no competing interests.

Open Access This article is licensed under a Creative Commons Attribution 4.0 International License, which permits use, sharing, adaptation, distribution and reproduction in any medium or format, as long as you give appropriate credit to the original author(s) and the source, provide a link to the Creative Commons licence, and indicate if changes were made. The images or other third party material in this article are included in the article’s Creative Commons licence, unless indicated otherwise in a credit line to the material. If material is not included in the article’s Creative Commons licence and your intended use is not permitted by statutory regulation or exceeds the permitted use, you will need to obtain permission directly from the copyright holder. To view a copy of this licence, visit <http://creativecommons.org/licenses/by/4.0/>.

References

- Beusen AHW, Van Beek LPH, Bouwman AF, Mogollón JM, Middelburg JJ (2015) Coupling global models for hydrology and nutrient loading to simulate nitrogen and phosphorus retention in surface water-description of IMAGE-GNM and analysis of performance. *Geosci Model Dev* 8:4045–4067
- Beusen AHW, Bouwman AF, Van Beek LPH, Mogollón JM, Middelburg JJ (2016) Global riverine N and P transport to ocean increased during the 20th century despite increased retention along the aquatic continuum. *Biogeosciences* 13:2441–2451

- Beusen, AHW, Bouwman AF (2022) Future projections of river nutrient export to the global coastal ocean show persisting nitrogen and phosphorus distortion. *Front. Water* 4
- Beusen AHW, Doelman JC, Van Beek LPH, Van Puijenbroek PJTM, Mogollón JM, Van Grinsven HJM, Stehfest E, Van Vuuren DP, Bouwman AF (2022) Exploring river nitrogen and phosphorus loading and export to global coastal waters in the shared socioeconomic pathways. *Glob. Environ. Chang.* 72
- Bey I, Jacob DJ, Yantosca RM, Logan JA, Field BD, Fiore AM, Li Q, Liu HY, Mickley LJ, Schultz MG (2001) Global modeling of tropospheric chemistry with assimilated meteorology: model description and evaluation. *J Geophys Res Atmos* 106:23073–23095
- Bidoglio GA, Mueller ND, Kastner T (2023) Trade-induced displacement of impacts of global crop production on oxygen depletion in marine ecosystems. *Sci Total Environ* 873:162226
- Bjørn A, Chandrakumar C, Boulay A-M, Doka G, Fang K, Gondran N, Hauschild MZ, Kerkhof A, King H, Margni M, McLaren S, Mueller C, Owsianiak M, Peters G, Roos S, Sala S, Sandin G, Sim S, Vargas-Gonzalez M, Ryberg M (2020a) Review of life-cycle based methods for absolute environmental sustainability assessment and their applications. *Environ Res Lett* 15:83001
- Bjørn A, Sim S, King H, Margni M, Henderson AD, Payen S, Bulle C (2020b) A comprehensive planetary boundary-based method for the nitrogen cycle in life cycle assessment: development and application to a tomato production case study. *Sci Total Environ* 715:136813
- Bjørn A, Sim S, King H, Patouillard L, Margni M, Hauschild MZ, Ryberg M (2020c) Life cycle assessment applying planetary and regional boundaries to the process level: a model case study. *Int J Life Cycle Assess* 25:2241–2254
- Boulay A-M, Bare J, Benini L, Berger M, Lathuilière MJ, Manzano A, Margni M, Motoshita M, Núñez M, Amandine, Pastor V, Ridoutt B, Oki T, Worbe S, Pfister S (2018) The WULCA consensus characterization model for water scarcity footprints: assessing impacts of water consumption based on available water remaining (AWARE). *Int J Life Cycle Assess* 23:368–378
- Breitburg D, Levin LA, Oschlies A, Grégoire M, Chavez FP, Conley DJ, Garçon V, Gilbert D, Gutiérrez D, Isensee K, Jacinto GS, Limburg KE, Montes I, Naqvi SWA, Pitcher GC, Rabalais NN, Roman MR, Rose KA, Seibel BA, Telszewski M, Yasuhara M, Zhang J (2018) Declining oxygen in the global ocean and coastal waters. *Science* (80-.)
- Cosme N, Hauschild MZ (2016) Effect factors for marine eutrophication in LCIA based on species sensitivity to hypoxia. *Ecol Indic* 69:453–462
- Cosme N, Hauschild MZ (2017) Characterization of waterborne nitrogen emissions for marine eutrophication modelling in life cycle impact assessment at the damage level and global scale. *Int J Life Cycle Assess* 22:1558–1570
- Cosme N, Mayorga E, Hauschild MZ (2018) Spatially explicit fate factors of waterborne nitrogen emissions at the global scale. *Int J Life Cycle Assess* 23:1286–1296
- Diaz RJ, Rosenberg R (2008) Spreading dead zones and consequences for marine ecosystems. *Science*. 80(321):926–929
- EC-JRC (2010) International Reference Life Cycle Data System (ILCD) handbook -- general guide for life cycle assessment -- detailed guidance, constraints. European Commission - Joint Research Centre - Institute for Environment and Sustainability
- ERSI (2020) ArcGIS Pro v.2.6.2
- Hauschild MZ, Huijbregts MAJ (2015) Life cycle impact assessment. Springer Press, pp 1–16
- Henderson AD, Niblick B, Golden HE, Bare JC (2021) Modeling spatially resolved characterization factors for eutrophication potential in life cycle assessment EPA Public Access. *Int J Life Cycle Assess* 26:1832–1846
- Henryson K, Hansson PA, Sundberg C (2018) Spatially differentiated midpoint indicator for marine eutrophication of waterborne emissions in Sweden. *Int J Life Cycle Assess* 23:70–81
- Johnson MD, Scott JJ, Leray M, Lucey N, Bravo LMR, Wied WL, Altieri AH (2021) Rapid ecosystem-scale consequences of acute deoxygenation on a Caribbean coral reef. *Nat Commun* 12:1–12
- Jwaideh MAA, Sutanudjaja EH, Dalin, Carole (2022) Global impacts of nitrogen and phosphorus fertiliser use for major crops on aquatic biodiversity. *Int J Life Cycle Assess* 27:1058–1080
- Lehner B, Döll P (2004) Development and validation of a global database of lakes, reservoirs and wetlands. *J Hydrol* 296:1–22
- Liu X, Dunne JP, Stock CA, Harrison MJ, Adcroft A, Resplandy L (2019) Simulating water residence time in the coastal ocean: a global perspective. *Geophys Res Lett* 46:13910–13919
- Messenger ML, Lehner B, Grill G, Nedeva I, Schmitt O (2016) Estimating the volume and age of water stored in global lakes using a geo-statistical approach. *Nat. Commun.* 7
- Morelli B, Hawkins TR, Niblick B, Henderson AD, Golden HE, Compton JE, Cooter EJ, Bare JC (2018) Critical review of eutrophication models for life cycle assessment. *Environ Sci Technol* 52:9562–9578
- Mutel C (2017) Brightway: an open source framework for life cycle assessment. *J Open Source Softw* 2:236
- Mutel C, Liao X, Patouillard L, Bare J, Fantke P, Frischknecht R, Hauschild M, Jolliet O, Maia de Souza D, Laurent A, Pfister S, Verones F (2019) Overview and recommendations for regionalized life cycle impact assessment. *Int J Life Cycle Assess* 24:856–865
- Natural Earth (2023) Ocean - free vector and raster map data [WWW Document]. <https://www.naturalearthdata.com/downloads/10m-physical-vectors/10m-ocean/> (accessed 5.17.23)
- Payen S, Cosme N, Alexander, Elliott H (2021) Freshwater eutrophication: spatially explicit fate factors for nitrogen and phosphorus emissions at the global scale. *Int J Life Cycle Assess* 26:388–401
- Philip S, Martin RV, Keller CA (2016) Sensitivity of chemistry-transport model simulations to the duration of chemical and transport operators: a case study with GEOS-Chem v10–01. *Geosci Model Dev* 9:1683–1695
- Richardson K, Steffen W, Lucht W, Bendtsen J, Cornell SE, Donges JF, Drüke M, Fetzer I, Bala G, von Bloh W, Feulner G, Fiedler S, Gerten D, Gleeson T, Hofmann M, Huiskamp W, Kummer M, Mohan C, Nogués-Bravo D, Petri S, Porkka M, Rahmstorf S, Schaphoff S, Thonicke K, Tobian A, Virkki V, Wang-Erlandsson L, Weber L, Rockström J (2023) Earth beyond six of nine planetary boundaries. *Sci. Adv.* 9
- Rockström J, Steffen W, Noone K, Persson Å, Chapin FS, Lambin EF, Lenton TM, Scheffer M, Folke C, Schellnhuber HJ, Nykvist B, de Wit CA, Hughes T, van der Leeuw S, Rodhe H, Sörlin S, Snyder PK, Costanza R, Svedin U, Falkenmark M, Karlberg L, Corell RW, Fabry VJ, Hansen J, Walker B, Liverman D, Richardson K, Crutzen P, Foley JA (2009) A safe operating space for humanity. *Nature* 461:472–475
- Rockström J, Gupta J, Qin D, Lade SJ, Abrams JF, Andersen LS, Armstrong McKay DI, Bai X, Bala G, Bunn SE, Ciobanu D, DeClerck F, Ebi K, Gifford L, Gordon C, Hasan S, Kanie N, Lenton TM, Loriani S, Liverman DM, Mohamed A, Nakicenovic N, Obura D, Ospina D, Prodan K, Rammelt C, Sakschewski B, Scholtens J, Stewart-Koster B, Tharammal T, van Vuuren D, Verburg PH, Winkelmann R, Zimm C, Bennett EM, Bringezu S, Broadgate W, Green PA, Huang L, Jacobson L, Ndehedehe C, Pedde S, Rocha J, Scheffer M, Schulte-Uebbing L, de Vries W, Xiao C, Xu C, Xu X, Zafra-Calvo N, Zhang X (2023) Safe and just Earth system boundaries. *Nat.* 1619
- Rockstrom et al (2023) Supplementary information Safe and just Earth system boundaries
- Rosenbaum RK, Anton A, Bengoa X, Bjørn A, Brain R, Bulle C, Cosme N, Dijkman TJ, Fantke P, Felix M, Geoghegan TS, Gottesbüren B,

- Hammer C, Humbert S, Jolliet O, Juraske R, Lewis F, Maxime D, Nemecek T, Payet J, Räsänen K, Roux P, Schau EM, Sourisseau S, van Zelm R, von Streit B, Wallman M (2015) The Glasgow consensus on the delineation between pesticide emission inventory and impact assessment for LCA. *Int J Life Cycle Assess* 20:765–776
- Roy PO, Azevedo LB, Margni M, van Zelm R, Deschênes L, Huijbregts MAJ (2014) Characterization factors for terrestrial acidification at the global scale: a systematic analysis of spatial variability and uncertainty. *Sci Total Environ* 500–501:270–276
- Roy PO, Huijbregts M, Deschênes L, Margni M (2012) Spatially-differentiated atmospheric source-receptor relationships for nitrogen oxides, sulfur oxides and ammonia emissions at the global scale for life cycle impact assessment. *Atmos. Environ*
- Ryberg MW, Owsianiak M, Clavreul J, Mueller C, Sim S, King H, Hauschild MZ (2018) How to bring absolute sustainability into decision-making: an industry case study using a planetary boundary-based methodology. *Sci Total Environ* 634:1406–1416
- Schulte-Uebbing L, Beusen AHW, Bouwman AF, De Vries W (2022a) From planetary to regional boundaries for agricultural nitrogen pollution. *Nature* 610:507
- Schulte-Uebbing LF, Beusen AHW, Bouwman AF, de Vries W (2022b) Supplementary Material: From planetary to regional boundaries for agricultural nitrogen pollution. *Nature* 610:507–512
- Steffen W, Richardson K, Rockström J, Cornell SE, Fetzer I, Bennett EM, Biggs R, Carpenter SR, De Vries W, De Wit CA, Folke C, Gerten D, Heinke J, Mace GM, Persson LM, Ramanathan V, Rayers B, Sörlin S (2015) Planetary boundaries: guiding human development on a changing planet. *Science* (80): 347
- Sutanudjaja EH, van Beek LPH, Drost N, de Graaf IEM, de Jong K, Peßenteiner S, Straatsma MW, Wada Y, Wanders N, Wissler D, Bierkens MFP (2018) PCR-GLOBWB 2.0: a 5 arc-minute global hydrological and water resources model. *Geosci Model Dev* 11:2429–2453
- UNEP (2019) Global guidance on environmental life cycle impact assessment indicators Volume 2
- Van Dingenen R, Dentener F, Crippa M, Leitao J, Marmer E, Rao S, Solazzo E, Valentini L (2018) TM5-FASST: a global atmospheric source-receptor model for rapid impact analysis of emission changes on air quality and short-lived climate pollutants. *Atmos Chem Phys* 18:16173–16211
- Vea EB, Bendtsen J, Richardson K, Ryberg M, Hauschild M (2022) Spatially differentiated marine eutrophication method for absolute environmental sustainability assessments. *Sci. Total Environ.* 843
- Verones F, Hellweg S, Antón A, Azevedo LB, Chaudhary A, Cosme N, Cucurachi S, de Baan L, Dong Y, Fantke P, Golsteijn L, Hauschild M, Heijungs R, Jolliet O, Juraske R, Larsen H, Laurent A, Mutel CL, Margni M, Núñez M, Owsianiak M, Pfister S, Ponsioen T, Preiss P, Rosenbaum RK, Roy PO, Sala S, Steinmann Z, van Zelm R, Van Dingenen R, Vieira M, Huijbregts MAJ (2020) LC-IMPACT: a regionalized life cycle damage assessment method. *J Ind Ecol* 24:1201–1219
- Wang J, Song C, Reager JT, Yao F, Famiglietti JS, Sheng Y, MacDonald GM, Brun F, Schmied HM, Marston RA, Wada Y (2018) Recent global decline in endorheic basin water storages. *Nat. Geosci.* 11:926–932
- Wowra K, Zeller V, Schebek L (2020) Nitrogen in life cycle assessment (LCA) of agricultural crop production systems: comparative analysis of regionalization approaches. *Sci. Total Environ.* 143009
- Zhou J, Scherer L, van Bodegom PM, Beusen A, Mogollón JM (2022) Regionalized nitrogen fate in freshwater systems on a global scale. *J Ind Ecol* 26:907–922

Publisher's Note Springer Nature remains neutral with regard to jurisdictional claims in published maps and institutional affiliations.